Computers and Structures 321 (2026) 108040

Contents lists available at ScienceDirect

Computers and Structures

journal homepage: www.elsevier.com/locate/compstruc

Experimental and numerical investigation of tramcar curve squeal under varying wheel-rail contact conditions☆

Federico Castellini [a,*], Leonardo Faccini [a], Stefano Alfi [a], Egidio Di Gialleonardo [a], Roberto Corradi [a], Giacomo Squicciarini [b], David Thompson [b]

[a] Department of Mechanical Engineering, Politecnico di Milano, Via Giuseppe La Masa 1, 20156 Milano, Italy
[b] ISVR, University of Southampton, Southampton SO17 1BJ, United Kingdom

ARTICLE INFO

Keywords:
Curve squeal
Noise measurements
Vehicle dynamics
Wheel-rail contact
Stability analysis
Frequency-domain simulations
Tramways

ABSTRACT

The variability of curve squeal generated by a modern articulated tramcar is investigated through noise and vibration measurements at two sites and numerical simulations. Accelerometers on the leading wheels of the second car show that different vibration modes intermittently dominate the wheel vibration during curving, with squeal also detected on the outer wheel. To study low-adhesion conditions, the track is artificially wetted. A reduction of nearly 15 dBA in Single Event Levels is obtained after water application, but the effect disappeared after a few passes. A numerical procedure supports the experiments, combining vehicle dynamics simulations with a frequency-domain wheel-rail interaction model. Predicted squeal frequencies agree with those measured. Variability in contact parameters is considered by simulating numerous variants per scenario. Squeal occurs in over 90% of cases on the front inner and rear outer wheels, and in fewer than 3% on the outer front wheel. Simulations with varying friction coefficients are aligned with experimental findings in dry and wet conditions, suggesting that water-based friction modifiers can significantly reduce squeal. A parametric study on curve radius confirms the leading inner wheel as most critical, while also showing multiple squealing wheels, including those under flange contact.

1. Introduction

Curve squeal is a loud, tonal noise that commonly arises when a rail vehicle negotiates tight curves and is often perceived as highly disturbing by nearby residents. In densely populated areas, this phenomenon represents a significant issue, impacting thousands of people daily [1]. Over the years, various numerical and experimental studies have focused on investigating the phenomenon to identify its causes and potential mitigation solutions. A comprehensive literature review is provided by Thompson et al. in [2]. Different mechanisms have been proposed to describe the root causes of the physical phenomenon. Curve squeal is often attributed to the wheel-rail self-excitation caused by the falling behaviour of the friction curve in fully sliding conditions [1,3–5]. This is equivalent to a negative damping introduced into the system which, if it exceeds the structural damping of the coupled wheel-rail system, promotes instability. Another possible cause of instability is related to coupling phenomena between two modes of the wheel [6–9] or between the wheel and the rail dynamics [10–12], driven by the contact forces acting in normal and tangential directions.

Squeal simulations can be carried out using either frequency- or time-domain formulations. In the former, the system is linearised considering small fluctuations in the friction force about the steady-state curving condition and the stability of the linearised system is studied to determine potential unstable frequencies. In the latter, the nonlinear equations are solved directly in the time domain. The frequency-domain approach first proposed by Heckl [13,14] was extended by De Beer et al. in [15] including the wheel and the rail dynamics in the vertical direction. This formulation has been further developed by Huang [3,4] and Squicciarini et al. [16,17] to consider also longitudinal and spin dynamics and the presence of multiple contact points between the wheel and the rail. These mobility-based methods allow for the analysis of the stability of the coupled wheel–rail system by focusing on the behaviour at the contact points. In this case, system stability is assessed using the generalized Nyquist criterion for Multiple-Input and Multiple-Output

☆ This article is part of a special issue entitled: 'RAILWAYS 2024 (CAS)' published in Computers and Structures.

* Corresponding author.
E-mail address: federico.castellini@polimi.it (F. Castellini).

https://doi.org/10.1016/j.compstruc.2025.108040
Received 19 May 2025; Accepted 9 November 2025
Available online 29 November 2025

(MIMO) systems. [18,19]. Alternatively, the entire system can be modelled using Finite Element (FE) methods, as proposed in [20–23]. Similar FE-based approaches can be found in [24,25] for the detailed evaluation of wheel-rail wear and profile evolution. The main advantage of mobility-based methods lies in their computational efficiency, as full FE models require the inversion of very large matrices, particularly when a long and finely discretized model is used to represent track dynamics. Moreover, these approaches allow for a hybrid formulation of the system dynamics; for example, using a finite element model for the wheel and analytical or semi-analytical models for the rail, which significantly reduces computational cost. On the other hand, the key advantage of full FE models is that they allow the use of Complex Eigenvalue Analysis (CEA) for stability assessment, which enables the tracking of individual system eigenvalues as specific parameters vary. However, both modelling approaches have proven effective in predicting the occurrence of curve squeal.

Several time-domain approaches have been proposed. Curve squeal has been analysed through a simplified single degree of freedom modal model including only the lateral dynamics of the wheel [26–30] or accounting for the vertical-lateral coupling [6–8,31]. Comprehensive time-domain models for the wheel-rail interaction considering the longitudinal and the spin dynamics were also formulated by including the wheel and the rail dynamics through their mass, stiffness and damping matrices [3,32,33] or relying on Green's functions to increase the computational efficiency [12,34–37].

Both frequency- and time-domain investigations demonstrate that curve squeal arises when there is a high relative yaw angle between the wheelset and the rails (commonly known as the wheel-rail angle of attack). This misalignment creates a relative sliding velocity between the two bodies in contact (which is usually normalized by the vehicle speed and named creepage in rail applications), which can lead to self-excited vibrations responsible for the characteristic curve squeal noise [1]. This is why the leading axle of the vehicle, which is usually characterized by the highest value of angle of attack, is commonly the most critical for squeal occurrence [2]. Squeal is typically generated by the inner leading wheel, in proximity to the natural frequencies of the wheel axial and radial modes [1,2] but is also observed on the outer wheel [6,38,39]. In addition to the angle of attack, wheel squeal is further promoted by a high value of the friction coefficient between the wheel and the rail [1,2].

The impact of the contact angle and spin creepage are investigated in [37] through time-domain simulations. While the impact of the spin creepage is found to cause a minor variation in squeal and contact force amplitudes, the contact angle directly affects the wheel-rail dynamic coupling. A variation in the contact angle can suppress or promote the phenomenon, having a significant impact on its amplitude and/or on the wheel modes involved. This is also shown in [6]. Similarly, the presence of an additional contact between the back of the wheel flange and the groove rail on the inner leading wheel is found to alter the squealing frequencies and the wheel modes involved in the phenomenon [16,17,40]. The effect of longitudinal creepage is investigated in [20,41] through test rig experiments and numerical simulations, showing that an increase of the longitudinal creep can effectively mitigate squeal occurrence. According to these results, the numerical investigation carried out in [42] shows that a solid axle architecture may be beneficial in mitigating curve squeal compared to independently rotating wheels, thanks to the longitudinal differential slip developed in sharp curves due to solid axles.

Some experiments highlight that curve squeal can be effectively mitigated using water or friction modifiers applied on the track [43]. Tests presented with friction modifiers applied on top of the rail head (see [44,45]) have shown to be very effective in removing squeal. However, other test rig experiments reveal that curve squeal may still exist when friction modifiers are applied to eliminate the negative slope in the friction curve [27,29]. Other possible strategies to mitigate curve squeal may involve the use of wheel and rail dampers, adopting passive or active solutions to reduce the wheel-rail angle of attack (passive or active bogie steering) or using non-symmetric wheel and rail profiles to modify the position of the contact point between the wheel and the rail (these solutions are described in [1]). The potential for reducing curve squeal through active control was more recently investigated in [12], showing that curve squeal can be efficiently eliminated applying forced vibration to the vibrational system.

All the experimental and numerical findings reveal that curve squeal exhibits significant variability due to small changes in wheel-rail contact conditions, rendering the phenomenon highly unpredictable in some instances. These factors may vary significantly depending on the environmental conditions, the presence of dirt and third body layer or due to the wear of the wheel and rail profiles. During the curve negotiation, contact conditions may also experience slight variations due to the differences in the track alignment caused by position tolerances in the track gauge. Thus, curve squeal predictions performed adopting a specific friction coefficient or fixed wheel-rail contact condition may differ with respect to what highlighted in measurements. A comprehensive curve squeal prediction should consider all the possible sources of uncertainty in the wheel-rail contact conditions. To include contact variability into curve squeal simulations, a statistical approach has been adopted in [16,17,40,42,46]. Hundreds of curve squeal simulations are carried out by systematically varying wheel-rail contact conditions with respect to the ones identified in a vehicle dynamics simulation adopting nominal wheel and rail profiles. Other approaches are based on the sensitivity analysis or the most critical parameters such as contact angle, lateral contact point position and friction coefficient [4,5,7,8,26–30,32,35–37].

The objective of this research is to extend the analysis of the experimental findings previously presented in [38,43,46], which revealed substantial variability in curve squeal occurrence. The results of these experimental campaigns are collected here and further analysed. In addition to the results presented in [46], curve squeal noise measurements on a wet track are shown and a comprehensive numerical investigation is carried out. The numerical approach developed in [17,42] is used to extend the analysis performed on the leading axle of the leading car to the other wheels of the vehicle and to investigate curve squeal occurrence in different wheel-rail contact conditions. The impact of track misalignment and friction conditions is numerically evaluated to explain the experimental evidence. The squealing behaviour of the analysed tramcar is then assessed by varying the curve radius through a series of vehicle dynamics simulations combined with the high-frequency wheel-rail interaction model. The paper is organized as follows. Noise and vibration measurements for a tramcar experiencing different wheel-rail contact conditions are reported in Section 2. The modelling approach adopted to predict the squeal occurrence is introduced in Section 3. The results of the simulations are presented in Section 4 and final comments are provided in the concluding section.

2. Noise and vibration measurements

Over the past decade, the authors conducted several experimental campaigns analysing tram squeal noise under varying conditions. On-track measurements showed high variability, even in similar environments. Squeal was more frequent on dry rails but also occurred shortly after rain during drying [2]. Friction modifiers like lubricants and water proved effective in suppressing squeal [38]. However, squeal variability isn't only due to friction or environmental factors. Trams of the same model did not always produce consistent squealing frequencies under similar conditions [17]. Research showed that wear of wheel and rail profiles, and track construction tolerances, alter contact conditions, causing intermittent squeal and frequency shifts.

Curve squeal noise and vibration measurements at two different sites are reported here to highlight the variability of the phenomenon and its dependence on the wheel-rail contact conditions. Different squealing frequencies were observed not only across the different tests but even during the negotiation of a single curve. This analysis aims to

demonstrate that even minor changes in the wheel-rail contact conditions can lead to different squealing phenomena. All the measurements presented refer to curve negotiation at a constant speed (10 km/h) by modern low floor articulated tramcars with identical architectures. Each unit consists of seven carbodies, four mounted on individual bogies and three suspended between them. The vehicles operated on typical tramway tracks with grooved rails. The curve radii were 17.5 m at site 1 and 24 m at site 2.

2.1. Noise and vibration measurements at site 1 (curve radius 17.5 m)

The experimental campaign at site 1 involved both noise and vibration measurements. Track-side microphones were used to measure the noise emitted by the entire tramcar, while accelerometers were installed on the tyre of the leading inner and outer resilient wheels of the second bogie of the vehicle. Two single-axis accelerometers are mounted to measure vibration of the wheel rim in the axial and radial directions. The accelerometers are mounted side by side at a radial distance of 310 mm from the wheel centre. The signals measured by the accelerometers are transmitted to the onboard acquisition system via a telemetry system. To enable synchronization between the onboard and track-side measurements, an analog radio signal was acquired by both systems.

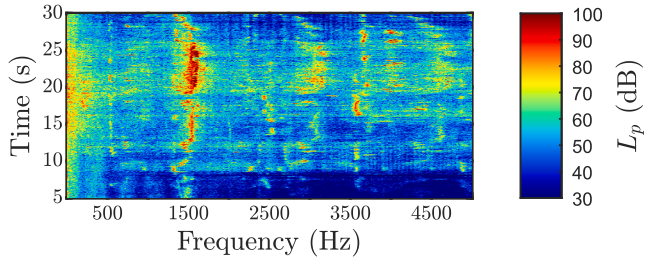

Fig. 1. Spectrogram of SPL measured at site 1 (microphone placed on the inner side of the curve at 2.5 m from track centre, $p_{ref} = 2{\cdot}10^{-5}Pa$) [46].

Since the track-side microphones capture the noise from all the wheels, it is not immediately clear whether the observed squealing frequencies should be attributed to a single wheel or multiple wheels that are squealing simultaneously. The accelerometers allow for isolating the contribution of a single wheel to the overall squeal. Further details of the experimental setup can be found in [38]. Fig. 1 presents an example of the spectrogram of the noise emitted by the tramcar during curve negotiation. Sound pressure was recorded by a microphone placed on the inner side of the curve, 2.5 m from track centreline. A strong noise emission is observed near 1500 Hz with a more intermittent tonal contribution around 2500 Hz and between 3300 and 3800 Hz. These tonal components in the spectrogram are less persistent than the one at 1500 Hz.

The analysis is further refined by evaluating the vibration of the wheel rim in both the axial and radial directions (Fig. 2). The spectrogram of the wheel acceleration (Fig. 2a) reveals distinct peaks in the vibration levels along both axial and radial directions, specifically near 1500 Hz, 2500 Hz, 3300 Hz and 3800 Hz. In this case, the presence of multiple tonal contributions is more apparent compared to the analysis conducted using the microphone. Additionally, tonal wheel vibration at 550 Hz is observed for a brief period at curve entrance and curve exit.

An Experimental Modal Analysis (EMA) was performed on the resilient wheel of these tramcars. The results were used to calibrate the wheel FE model developed for numerical simulations. These results are also reported in Appendix A (see also [17] for further details on the FE model). The vibration peaks observed in Fig. 2a are very close to the natural frequencies of the wheel axial mode with 2 Nodal Diameters (ND) at 535 Hz, the wheel axial and radial modes with 3 ND (1273 Hz and 1423 Hz), the wheel axial and radial modes with 4 ND (2230 Hz and 2479 Hz), the wheel axial and radial modes with 5 ND (3367 Hz and 3736 Hz) and the wheel axial mode with 6 ND (5112 Hz). These findings align with the experimental and numerical evidence also reported in the literature, where curve squeal is usually found near the natural frequencies of the wheel axial modes and occasionally near those of the radial modes. It should be noted that the mode shapes of this resilient wheel are strongly coupled in the two directions, particularly at high frequencies [17].

The vibration signals are also processed by adopting the fast time

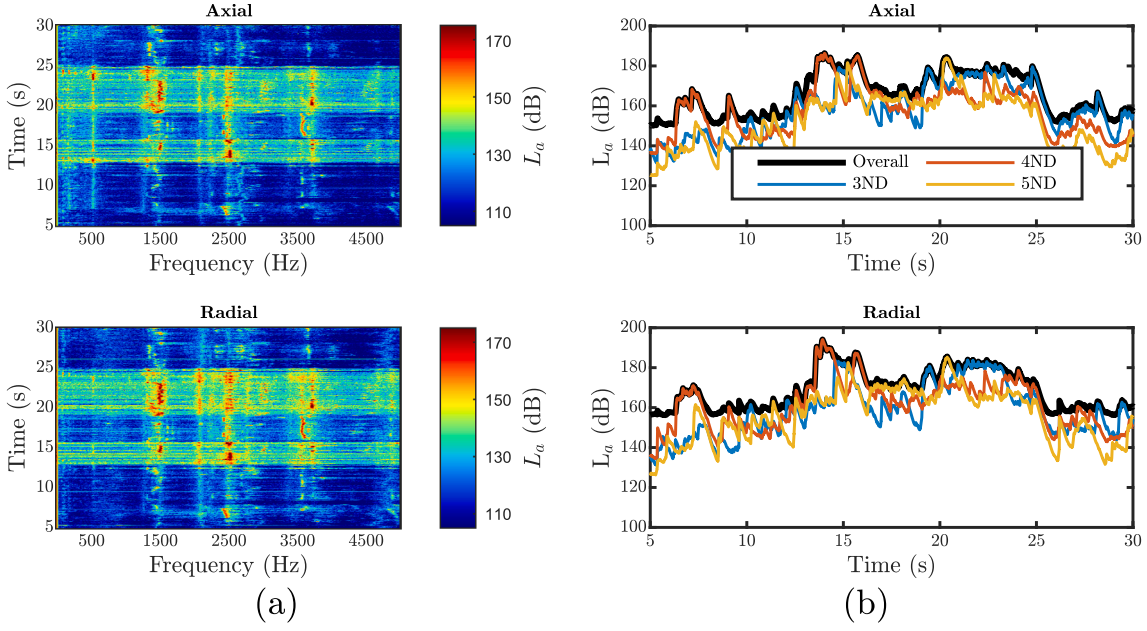

Fig. 2. Vibration measurements at site 1: (a) spectrograms and (b) fast time weighting of the inner wheel acceleration ($a_{ref} = 10^{-6}m/s^2$) in axial and radial directions [46].

Table 1
Wheel vibration modes and related frequency bands for the fast-weighting analysis.

Nodal Diameters (ND)	Wheel Modes	Frequency Range
2 ND	Axial (535 Hz)	440–707 Hz
3 ND	Axial (1273 Hz)	1130–1760 Hz
	Radial (1423 Hz)	
4 ND	Radial (2230 Hz)	1760–2825 Hz
	Axial (2479 Hz)	
5 ND	Radial (3367 Hz)	3150–4400 Hz
	Axial (3736 Hz)	
6 ND	Axial (5112 Hz)	4400–5650 Hz

weighting (the results are presented in Fig. 2b) [47]. In this case, the overall vibration level is compared with the level in specific frequency bands defined to isolate the main tonal contributions highlighted in the spectrograms. The list of the wheel modes involved in the squealing events and the frequency bands defined for the analysis are summarised in Table 1. Note that only the curves related to the contributions from the modes with 3, 4 and 5 ND are shown in Fig. 2b. This improves the diagram readability, as the contribution of other modes is not relevant during this specific squeal event.

While it might initially seem that multiple modes are simultaneously engaged in the squealing phenomenon when examining spectrograms, Fig. 2b underscores a distinct intermittent behaviour. This consistently reveals a single dominant frequency band in the overall wheel vibration, which varies at different time instances. This evidence suggests that multiple wheel modes can be involved in squeal during the negotiation of a specific curve; however, only a single mode dominates the limit cycle at any given time. This observation is typically also found in time-domain simulations, where a single vibration mode generally dominates the limit cycle [3,32,35].

The vibration measured by the accelerometers on the outer wheel is shown in Fig. 3. Tonal vibration is observed close to 1500 Hz during most of the curve negotiation. A tonal contribution at 2500 Hz is also detected for a brief time window at the curve entrance and exit. Similarly to what is observed on the inner wheel, the band analysis (Fig. 3b) shows that only one vibration mode dominates the limit cycle at a given time on the outer wheel as well.

2.2. Noise measurements at site 2 (curve radius 24 m) in case of dry and wet track

In this section, the results of another series of experiments are presented. The tests were conducted in another curve (site 2, radius R = 24 m) which is frequently affected by curve squeal. The squeal generated at this site by two tramcars with the same architecture but with different wheel profile wear has already been investigated in [17]. These results revealed quite dissimilar squealing patterns. The first tramcar generated squeal close to 550 Hz and 2500 Hz while the noise emitted by the second one was close to 1500 Hz and 2500 Hz (which is similar to what was observed also at site 1). The differences between the two were attributed to the presence of single and multiple contact points between the leading inner wheel of each bogie and the rail [17]. This article, however, presents an analysis of the effect of adhesion conditions on the curve, using a single tramcar. Pass-by noise is analysed by comparing different passages on dry track and artificially wetted track. The aim of the experiments was to recreate a low-adhesion situation to investigate the impact of the friction coefficient on curve squeal noise. It is important to note that during the experiments, it was not possible to accurately measure the exact amount of water present on the rails, ambient temperature, or humidity levels, all of which may affect evaporation. The same applies to the wheel-rail friction coefficient. Nevertheless, the results are still representative of the effects of using water (or water-based friction modifiers) on the occurrence of the phenomenon, effectively reproducing a range of high- (dry track) and low-adhesion (wet track) scenarios. A total of 12 passages of the same tramcar were conducted. The time window for two successive tram passages falls within a 6–8 min interval. The first 6 passages were performed on dry track, similarly to the previous measurements. The spectrogram of the noise levels recorded during the first passage by a microphone placed 2.5 m from the inner side of the track is shown in Fig. 4a. Just before the seventh passage, water was applied to both rails along the curve, and the tramcar completed six additional passages. The spectrogram of the noise levels during passage 7 is shown in Fig. 4b, indicating that the main tonal contributions at 550 Hz and 2500 Hz observed in passage 1 disappear in presence of water on the rail.

The comparison between the case of dry and wet track conditions confirms that wheels are less prone to squeal under low adhesion and

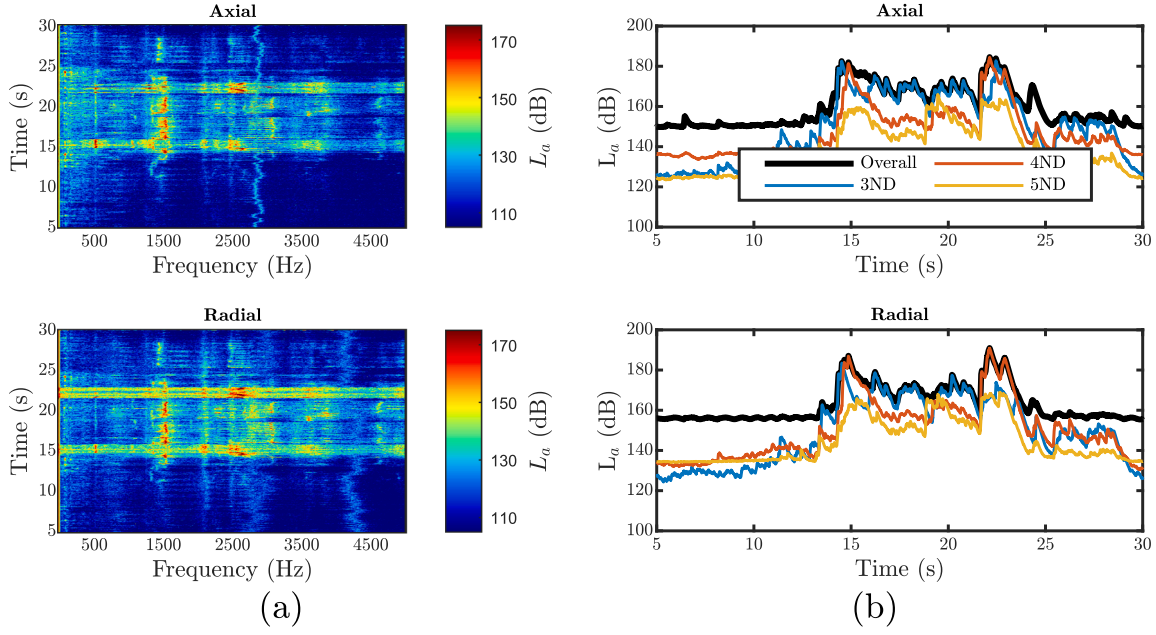

Fig. 3. Vibration measurements at site 1: (a) spectrograms and (b) fast time weighting of the outer wheel acceleration ($a_{ref} = 10^{-6} m/s^2$) in axial and radial directions [46].

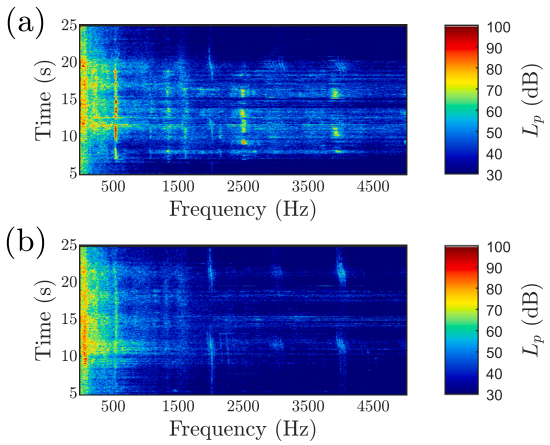

Fig. 4. Spectrogram of SPL measured in site 2 (microphone placed on the inner side of the curve at 2.5 m from track centre, $p_{ref} = 2{\cdot}10^{-5}Pa$: (a) passage 1, dry track and (b) passage 7, wet track.

demonstrates that water can completely suppress the occurrence of the phenomenon. A lower friction coefficient results in reduced tangential contact forces, which in turn decrease the lateral-vertical coupling responsible for mode-coupling mechanisms or the coupling between wheel modes and the rail. Furthermore, the effect of falling friction is less under wet conditions, as found by Polach through measurements on dry and wet tracks [48].

However, this result appears to contradict reports from some tram drivers, who often observe that the worst situation for curve squeal noise phenomena occurs immediately after heavy rain (this is also reported in [2]). To investigate this, the evolution of the noise emitted is considered over the different passages after the water was spread over the rails. The A-weighted spectra of the sound pressure recorded for each vehicle passage are presented in Fig. 5.

The overview of the effect of water application on curve squeal is provided in Fig. 6. Fig. 6a displays the average spectra of the noise SPL for three groups of passages: 1–6 (dry), 7–8 (wet), and 9–12 (post-wet). The results show that the effect of the water is limited to two passages then the noise levels and the tonal components in the spectrum return to the dry track values. The Single Event Levels (SEL) for each passage are also reported in Fig. 6b, indicating a reduction of nearly 15 dBA during passages 7–8, immediately following water application. Then the SEL increases (passages 9–12) and returns to the values also obtained in the case of dry track (passages 1–6) [49]. The analysis of the Single Event Level (SEL) also confirms the significant contribution of squeal noise to the overall noise emitted by the tramcar, highlighting the importance of identifying effective countermeasures to reduce noise exposure for inhabitants. These observations suggest that the low adhesion condition induced by water application is sufficient to suppress squeal directly after the treatment. However, as the track dries rapidly after only a few vehicle passages, the mitigating effect of water vanishes. This finding is consistent with previous numerical investigations, which indicate that curve squeal occurs once a threshold value of the friction coefficient is exceeded [2]. It is also in agreement with the experience of tramcar drivers who report that high levels of curve squeal may occur immediately after rainfall, as the beneficial effect of water appears to be limited to only a few vehicle passages. Furthermore, in the case of tramways with shared corridors, it should be noted that the rails are often contaminated by dirt and debris carried by road traffic. Rainfall can exert a cleaning effect of the rail surface, consequently, as the track

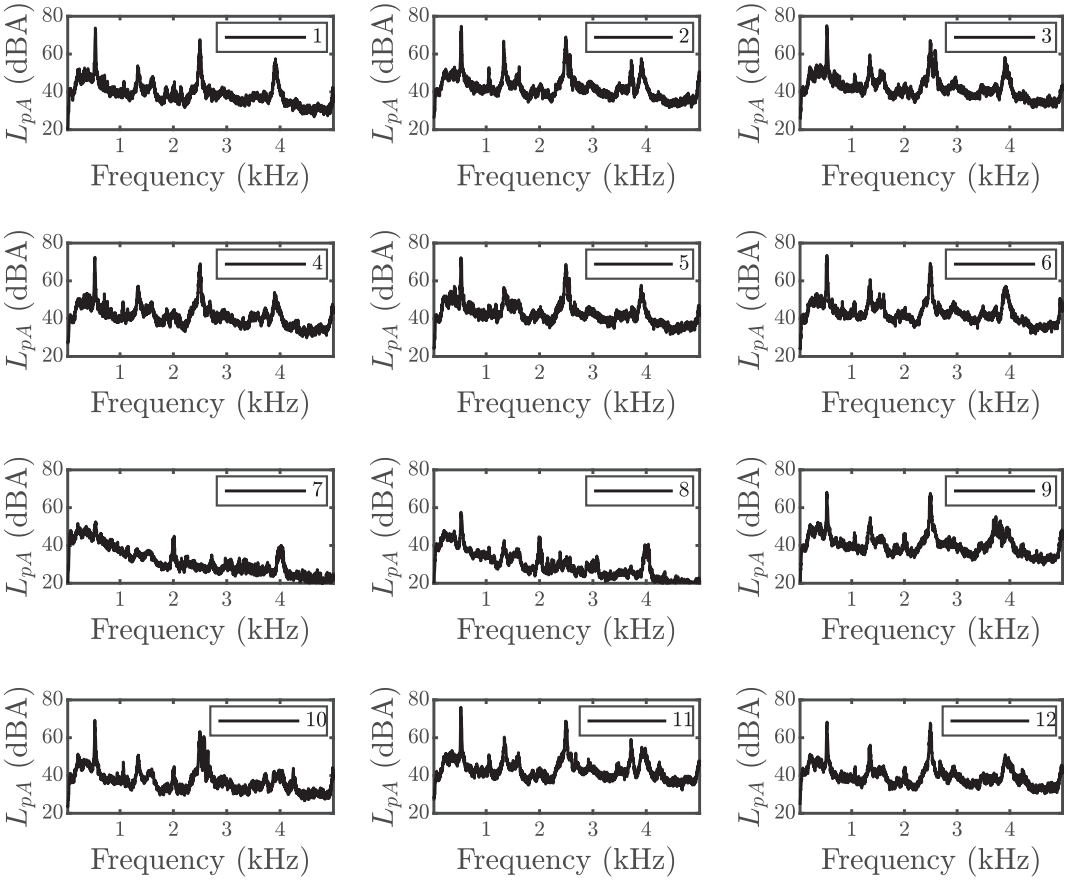

Fig. 5. Spectra of the SPL (dBA, $p_{ref} = 2{\cdot}10^{-5}Pa$) measured during each train passage (microphone placed on the inner side of the curve at 2.5 m from track centre).

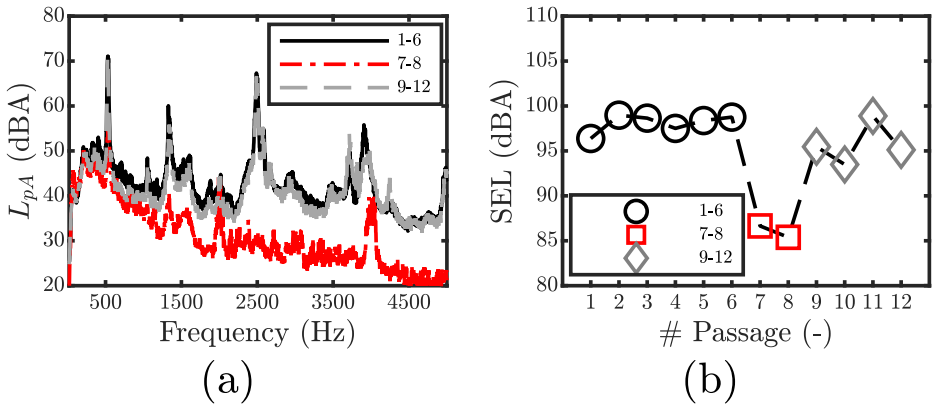

Fig. 6. Overview of the impact of the water on the rail: (a) average spectra of the noise levels for different series of vehicle passage (dBA, $p_{ref} = 2 \bullet 10^{-5} Pa$) and (b) Single Event Levels (SEL). Microphone placed on the inner side of the curve at 2.5 m from track centre.

dries, the average wheel-rail friction coefficient may surpass that recorded under dry conditions prior to the precipitation event.

3. Numerical investigation

Curve squeal prediction is conducted using a two-step numerical procedure as illustrated in Fig. 7. First, the vehicle's dynamics is simulated in the time domain to analyse the tramcar behaviour during curve negotiation. In the second step, squeal occurrence is assessed via a coupled wheel–rail model formulated in the frequency domain [17,42]. To this end, the vehicle dynamics is linearized about the steady-state curving condition. This enables the stability analysis of the coupled wheel–rail system with respect to that steady-state configuration, with system instability being indicative of the potential onset of squeal.

3.1. Multibody simulation of the tramcar running in curve

A multibody model is adopted to describe the vehicle dynamics during curve negotiation. This analysis is performed using a multibody simulation tool developed at the Department of Mechanical Engineering of Politecnico di Milano, which has been validated through experimental testing on various tramcar types [50–53]. The mathematical model has been designed to reproduce the dynamics of the whole tramcar during curve negotiation. The carbodies are modelled as rigid bodies and are interconnected by kinematic constraints and/or elastic and viscous elements, replicating the actual connections between them. The wheel-rail contact model is based on a multi-Hertzian approach [54,55] that enables the possibility of multiple simultaneous contact points. The effect of the rubber elements interposed between the tyre and the web in the resilient wheels is included through a truncated modal approach. The model is used to reproduce the characteristics of the vehicle and the geometry of the curves during the tests at site 1 and site 2 and then to carry out simulations varying the curve radius.

3.2. Curve squeal model

The prediction of curve squeal is carried out through a wheel-rail interaction model formulated in the frequency domain, where the wheel and the rail are coupled through a Hertzian spring and creep forces [42]. The non-linear equations of motion that describe the relative velocity between the wheel and the rail (wheel-rail sliding velocities) are linearised about the steady state curving condition defined in the multibody simulation. The formulation accounts for displacements in longitudinal, transverse and normal directions as well as spin rotation. The scheme of the wheel-rail coupled model is illustrated in Fig. 8a. $\mathbf{v^w} = [\,v_1^w \quad v_2^w \quad v_3^w \quad v_6^w\,]^T$ and $\mathbf{v^r} = [\,v_1^r \quad v_2^r \quad v_3^r \quad v_6^r\,]^T$ are the wheel and rail velocity in longitudinal, tangential and normal directions, and the spin rotation while k_H is the linearized Hertzian spring.

According to [1,3], the wheel-rail dynamics coupled by the contact forces is schematized as a MIMO system (see Fig. 8b), where $\mathbf{F} = [\,f_1 \quad f_2 \quad f_6\,]^T$ is the column matrix collecting the longitudinal and

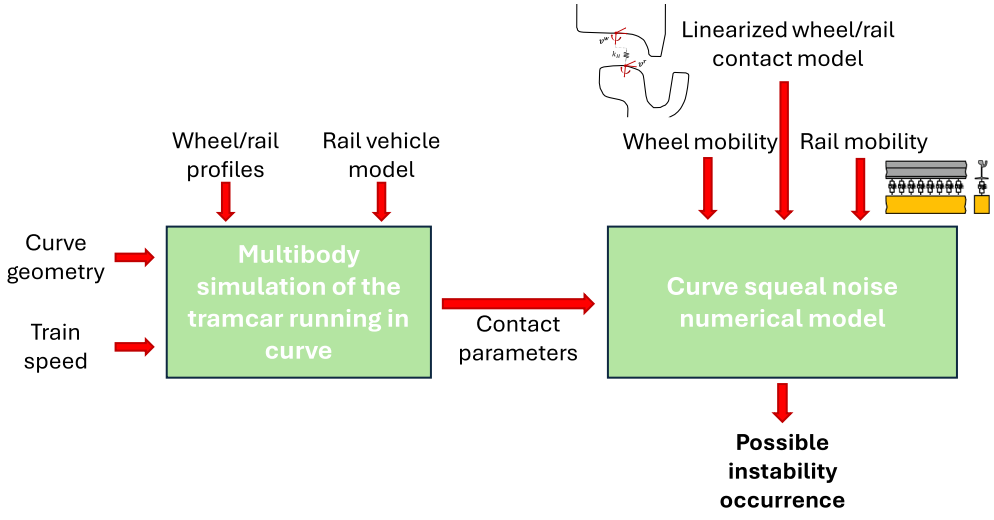

Fig. 7. Scheme of the methodology adopted to predict curve squeal occurrence [42].

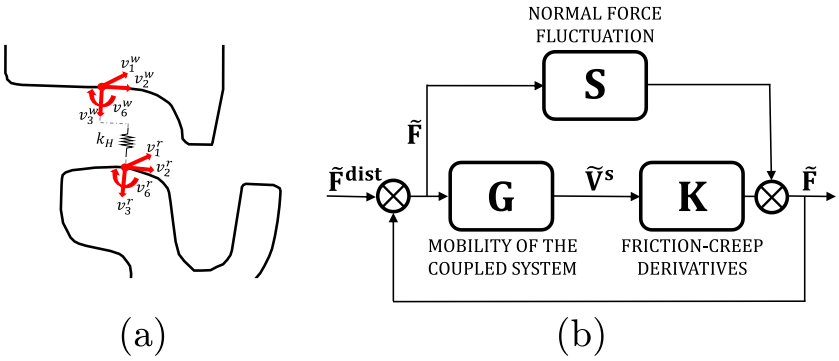

Fig. 8. Curve squeal model: (a) wheel-rail interaction and (b) scheme of the wheel-rail Multiple-Input and Multiple-Output (MIMO) loop.

transverse creep forces, and the spin moment, while $\mathbf{V^s} = \begin{bmatrix} v_1^s & v_2^s & v_6^s \end{bmatrix}^T$ collects the longitudinal, transverse and spin sliding velocities.

Matrix **G** is the mobility of the coupled system, defined as:

$$\mathbf{G} = \begin{bmatrix} Y_{11} - \frac{Y_{13}Y_{31}}{Y_{33}} & Y_{12} - \frac{Y_{13}Y_{32}}{Y_{33}} & Y_{16} - \frac{Y_{13}Y_{36}}{Y_{33}} \\ Y_{21} - \frac{Y_{23}Y_{31}}{Y_{33}} & Y_{22} - \frac{Y_{23}Y_{32}}{Y_{33}} & Y_{26} - \frac{Y_{23}Y_{36}}{Y_{33}} \\ Y_{61} - \frac{Y_{63}Y_{31}}{Y_{33}} & Y_{62} - \frac{Y_{63}Y_{32}}{Y_{33}} & Y_{66} - \frac{Y_{63}Y_{36}}{Y_{33}} \end{bmatrix} \tag{1}$$

where $Y_{ij} = Y_{ij}^w + Y_{ij}^r + Y_{ij}^c$ is the sum of the wheel, rail and contact mobilities.

Matrix **K** is a 3 by 3 matrix that relates the dynamic fluctuation in creep forces induced by a variation in creepages:

$$K_{ij} = \frac{f_{30}}{v_0}\frac{\partial \mu_i}{\partial \gamma_j} \qquad i,j = 1,2,6 \tag{2}$$

where f_{30} is the steady state normal load, v_0 is the vehicle speed while μ_i and γ_j are the adhesion coefficients (creep forces normalised against the normal load) and the creepages in the i,j-directions.

Matrix **S** is a 3 by 3 matrix defined as:

$$\mathbf{S} = -\mathbf{R}\begin{bmatrix} \frac{Y_{31}}{Y_{33}} & \frac{Y_{32}}{Y_{33}} & \frac{Y_{36}}{Y_{33}} \end{bmatrix} \tag{3}$$

where **R** is a 3 by 1 matrix that includes the effect of a fluctuation in the normal load on creep forces:

$$R_i = \mu_i + f_{30}\frac{\partial \mu_i}{\partial f_3} \qquad i = 1,2,6 \tag{4}$$

The detailed formulation of the wheel-rail interaction model, including the extended formulation used in case of multiple contact points between the wheel and the rail, can be found in [17,42].

The stability analysis is performed through the Nyquist Generalized Criterion for MIMO systems [1,18,19]. As introduced in Section 1, instability can be either induced by mode-coupling and falling friction. Mode-coupling instability is addressed by considering the dynamics of the wheel and the rail in the normal and transverse directions, on the other hand, falling friction is typically not integrated into tangential contact models. The tangential contact problem is solved using the model proposed by Polach [56] in which the falling friction effect is included in the calculation adopting an empirical formula that fits the slip-dependent friction behaviour observed during locomotive traction [48].

$$\mu(\gamma_{tot}) = \mu_0((1-A)e^{-B\gamma_{tot}v_0} + A) \tag{5}$$

$$\gamma_{tot} = \sqrt{\gamma_1^2 + \gamma_2^2} \tag{6}$$

where the slope of the friction curve is determined by the coefficients A and B, while μ_0 represents the static friction coefficient and γ_{tot} (Eq. (6)) is the total creepage. Alternative methods to include a slip-dependent friction coefficient in the calculations can be found in [3–5,57,58].

The wheel-rail interaction model is designed to reproduce the standard contact conditions between the leading inner wheel and the rail (tread contact, see Fig. 9a) as well as the presence of a second contact point between the wheel flange back and the check rail (Fig. 9b) or multiple contact points on the leading outer wheel (Fig. 9c).

The wheel dynamics is introduced through a finite element (FE) model of the resilient wheel mounted on the tramcar, while the rail dynamics is modelled by adopting an infinite Timoshenko beam on a viscoelastic foundation. The parameters of the models are calibrated based on the experimental Frequency Response Functions (FRFs) (see Appendix A).

4. Curve squeal simulations

Numerical simulations are presented in this section. First, the curve negotiation at site 1 (R = 17.5 m) and site 2 (R = 24 m) is simulated. The squealing behaviour of the tramcar is assessed under different wheel-rail contact conditions, simulating potential effects due to track misalignment or wheel and rail profile wear. For site 1, additional simulations are performed considering an increased track gauge (1447 mm) with

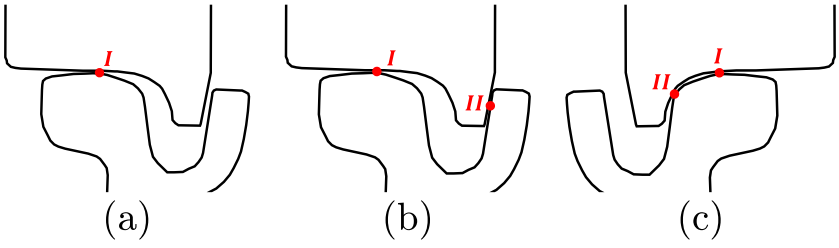

Fig. 9. Overview of potential wheel-rail contact conditions on the tramcar leading axle during a left-hand curve: (a) inner wheel, single contact point on the wheel tread, (b) inner wheel, multiple contacts on the wheel tread and on the flange back and (c) outer wheel, contacts on the wheel tread and on the wheel flange.

Table 2
Variability of the contact parameters in the squeal simulation.

Parameter	Symbol	Variation
Vehicle Speed	$v(kmh^{-1})$	
Normal Load	$F_{30}(kN)$	
Longitudinal Creepage	$\gamma_{10}(-)$	
Transverse Creepage	$\gamma_{20}(-)$	±20 %
Spin Creepage	$\gamma_{60}(-)$	
Contact Angle	$\theta(^\circ)$	
Lateral shift in CP* Position	$\Delta l_2(m)$	$[-0.005, 0.005]$
Friction Coefficient	$\mu(-)$	$[0.2, 0.7]$
Polach coefficient A	$A(-)$	$[0.1, 0.5]$
Polach coefficient B	$B(-)$	$[0.5, 1]$

* CP: Contact Point.

respect to the nominal value (1445 mm). This results in the activation of flange back contact on the inner wheels of the leading axles of each car and on the outer wheels of the trailing axles. All wheels of the vehicle are analysed to identify those most critical for the onset of squeal events and to determine whether simultaneous squealing events can occur on different wheels. Subsequently, site 2 simulations are conducted by varying the friction coefficient to consider the impact of adhesion conditions on squeal occurrence. Finally, a parametric investigation is carried out to investigate the squealing behaviour of the vehicle for different curve radii. Simulations are based on the methodology outlined in Section 3. The steady-state curving conditions are computed through a multibody simulation of the vehicle running along the curve at constant speed (10 km/h), as in the experiments. The analysis follows the procedure adopted in [17,42] to identify the most critical squeal-prone frequencies. A set of 200 simulations per scenario is generated by randomly varying the contact parameters within the ranges reported in Table 2. This approach allows the inclusion of the typical variability in wheel-rail contact conditions along the curve within the simulations. Such variations may arise from wheel-rail irregularities, profile wear or changes in environmental conditions. A large variability is included in the value of friction coefficient to consider also the most critical scenarios for curve squeal occurrence. The interval is limited to the friction coefficient measured on dry rail in [59].

The unstable frequencies identified for each simulated case are compared with the wheel mobility to assess if instability is associated with one or more wheel vibration modes. Furthermore, as performed in [42], the squeal occurrence percentage is calculated as the ratio between the number of unstable cases and the total number of simulations, evaluated within different one-third octave bands. This enables the identification of how critical a specific wheel vibration mode is relative to others, and how its unstable frequency is affected by local variations of wheel-rail contact conditions. This metric is also used to compare the squeal sensitivity of different wheels and to analyse how squeal occurrence evolves with varying curve radius.

4.1. Simulation of curve squeal occurrence in site 1

The results for the leading inner wheel at site 1 are presented in detail first (see Fig. 10). Unstable frequencies are indicated by red dots superimposed on the wheel mobility diagram, and the squeal occurrence percentage is reported below. The axial wheel mode with 2 ND (535 Hz) is the primary contributor to system instability, with a squeal occurrence of 99 %. Lower squeal occurrences are obtained for the wheel modes with 3 ND (1273 and 1423 Hz, 23 %) and 4 ND (2479 Hz, 35 %). A small number of unstable points cases is also associated with the wheel modes with 5 ND (3736 Hz, 1 %) and 6 ND (5112 Hz, 5 %).

Simulations are repeated for all the wheels of the vehicle, considering an increased track gauge (1447 mm) to investigate the impact of a change in the wheel-rail contact conditions on the leading inner and the outer trailing wheels. As far as the adhesion conditions are concerned,

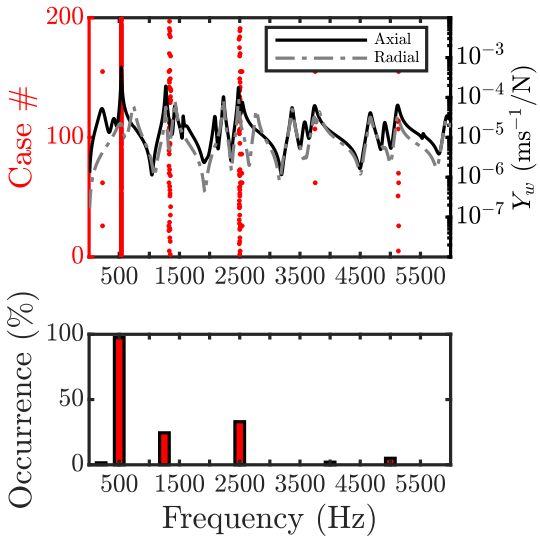

Fig. 10. Results of the curve squeal simulation: curve squeal occurrence (%) on the inner leading wheel (site 1, track gauge 1445 mm).

the same values for the friction coefficient and the falling friction parameters are adopted.

The increase in track gauge leads to the activation of an additional contact point between the flange back of the wheel and the rail (see Fig. 9b). As a result, the distribution of wheel-rail contact forces changes (further details can be found in [17]). This situation frequently occurs in practice on the reference tramcar, particularly in sharper curves, as is evident from significant wear on the check rails along the curve.

As observed in the simulations, it is sufficient to increase the track gauge by 1–2 mm to activate the contact between the flange back and the checkrail. Notably, a small load on the flange back (400 N) is also observed on the inner leading wheel of the last car even in the case of nominal track gauge. The adhesion level also plays a role in promoting flange back contact. When the friction coefficient is high, transverse creep forces increase, generating a counter-steering yaw moment on the bogie. This moment pushes the leading axle toward the outer rail and the trailing axle toward the inner rail. The resulting increase in lateral forces leads to greater deformation of the rubber elements in the resilient wheels, which causes additional relative lateral displacement between the wheels and the rails. Consequently, contact between the flange back and the checkrails is promoted. Thus, a higher friction coefficient can either activate flange back contact or increase the load on existing flange and/or flange back contacts.

While resilient wheels are included in the multibody simulation, the wear of wheel and rail profiles is not considered so the activation of this contact point is induced by introducing a small increase in the track gauge as performed in [17] (a 2 mm increase with respect to the nominal track gauge). The results of the two sets of simulations are reported in terms of squeal occurrence percentage in Fig. 11. For the first car, the most critical wheel is confirmed to be the leading inner one. In the case of nominal track gauge (black bar, ■), the leading inner wheel and the trailing outer wheel are in tread contact with the rail (this is common to the other cars, except for the leading inner wheel of the last car, as mentioned above). Squeal is found on both wheels involving the wheel axial mode with 2 ND and the ones with 3, 4 ND but with lower occurrence percentage. It must be noted that, in very sharp curves, the bogie is in a fully constrained condition, such that the trailing outer wheel experiences contact conditions very similar to those of the inner leading wheel [60]. This is due to the comparable creepage levels and contact force distributions between the inner leading and trailing outer wheels. On the other hand, the leading outer wheel and the trailing inner wheel, which are in flange contact conditions (see Fig. 9c), exhibit squeal only near 1500 Hz. A significantly lower percentage of squeal,

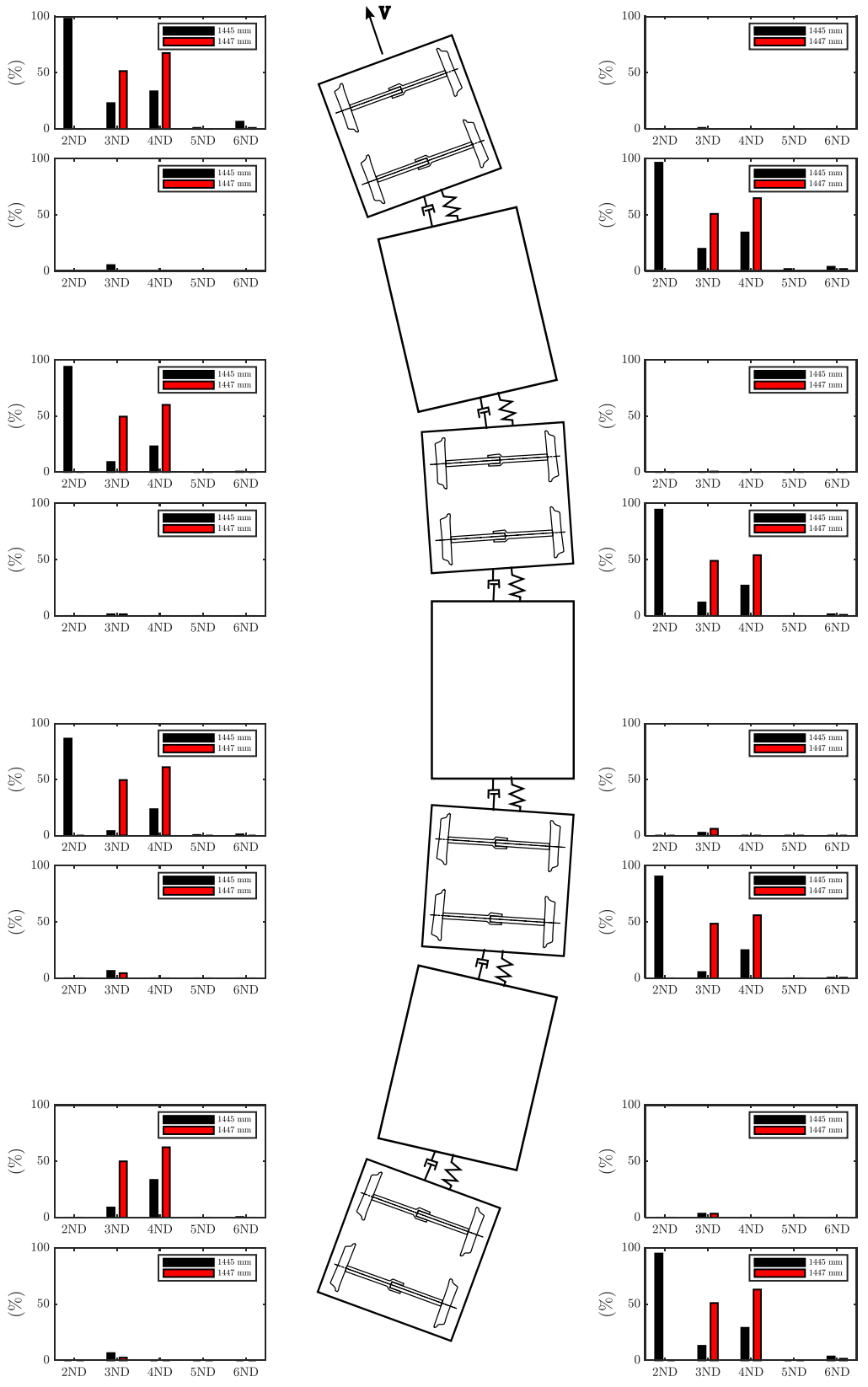

Fig. 11. Results of the squeal simulation of site 1 (R = 17.5 m) with different track gauge: (■) 1445 mm and (■) 1447 mm.

less than 3 %, is observed on the leading outer wheels compared to the leading inner wheels. A similar trend is detected when comparing the trailing inner and outer wheels. This suggests that specific contact conditions are required for squeal to occur in the case of flange contact, while squeal generated by the leading inner wheel, also in the presence of flange back contact, is more common. The squealing behaviour on the four wheels of a bogie is very similar across the different cars of the vehicle. These results may explain why multiple squealing frequencies are often observed simultaneously in track-side microphone spectrograms (see Fig. 1 and Fig. 4). These frequencies may arise not only from the intermittent nature of squeal on a single wheel, but also from simultaneous squealing on multiple wheels.

The results of the simulations with an increased track gauge (red bar, ■) reveal potential squealing frequencies that are close to those observed in site 1 measurements, where squeal was predominantly observed near 1500 Hz (corresponding to 3 ND) and 2500 Hz (4 ND) on the inner wheel and near 1500 Hz on the outer wheel on the leading axle of the second car. As highlighted in past research ([17]), the activation of the flange back contact completely alters the squeal occurrence. In the presence of flange back contacts, no squeal occurrence is detected for the axial mode with 2 ND, whereas higher squeal occurrence is obtained for the wheel vibration modes with 3 and 4 ND. These results highlight that, in sharp curves, it is possible that both the leading inner and the trailing outer wheel are squealing simultaneously, and the leading outer wheel may also contribute to squeal, as highlighted by measurements (see Section 2.1). As anticipated above, the leading inner wheel of the last car operates in a flange back contact condition even under nominal track gauge. In that case, similar squealing frequencies are found compared to the 1447 mm track gauge simulation. However, the squeal occurrence differs, revealing how even a change in the load on the flange back (from 400 N to 8.8 kN) can alter the squeal behaviour. Furthermore, while the 535 Hz squeal (associated with tread contact) is induced by falling friction, the squeal at 1500 Hz and 2500 Hz occurs even when a constant friction coefficient is imposed, as long as two contact points exist between the wheel and the rail. This suggests that the presence of two contact points promotes lateral-vertical dynamic coupling, leading to mode-coupling instability.

Table 3
Summary of the experimental and numerical results for site 1.

	Inner wheel	Outer wheel
Measurements	**1500, 2500**	**1500**, 2500*
Simulations (track gauge 1445 mm)	500, 2500, 1500	–
Simulations (track gauge 1447 mm)	**2500, 1500**	**1500**

* Squeal occurrence only at curve entrance and curve exit in short time windows.

These results suggest that, in some cases, it may be sufficient to analyse a single bogie (or even a single axle) to achieve an almost complete evaluation of tramcar squeal. This simplification is valid given that all the cars share similar architecture and wheel-rail contact conditions during curve negotiation. This situation is common for articulated tramcars equipped with bogies with the same design negotiating very sharp curves. However, if larger-radius curves are considered or vehicles with heterogeneous car architectures, contact conditions may vary considerably between wheels, potentially leading to different squeal characteristics. In such cases, a comprehensive characterization of the vehicle with respect to the squeal occurrence requires analysing the steady-state behaviour of all wheels.

A summary of the results from the experimental activities and numerical simulations is presented in Table 3. The squeal frequencies measured by microphones and accelerometers on the inner and outer wheels are reported. The squeal frequencies obtained from the numerical simulations are ranked by percentage of occurrence. This shows that the frequencies observed in the experimental measurements are among the most likely to squeal predicted by the numerical model, confirming the consistency between numerical predictions and measured data. This agreement is especially evident in the simulations results obtained for an increased track gauge (1447 mm), which closely match the experimental findings, as highlighted in bold in Table 3.

4.2. Simulation of curve squeal occurrence in site 2

The dry and wet wheel-rail contact conditions of the site 2 experiments are reproduced numerically by varying the friction coefficient. Different adhesion conditions are simulated by limiting the variation range of the friction coefficient, generating two sets of simulations with $\mu_0 = [0.1–0.3]$ and $\mu_0 = [0.3–0.7]$ for the wet and dry track respectively. The range of falling friction parameters A and B for the dry case is the same as that used in the Site 1 simulations. However, the traction curve measured in case of wet rail in [48] shows also a much less pronounced falling friction effect in the saturation area. This suggests that an adjustment in the B coefficient is needed to reproduce realistically wet track conditions. Therefore, since the coefficient B proposed by Polach in [48] for dry track (B = 0.6) is three times the value proposed for wet rails (B = 0.2), the parameter B used in the dry track simulations is scaled by a factor 3 for the wet rail simulations. This enables a more realistic comparison of the squeal generated by the tramcar in case of low and high adhesion conditions. Simulations are performed using a nominal track gauge (1445 mm). Only the results of the leading car are here reported. Similar, though slightly lower, squeal occurrence is observed on the other cars, such as shown in site 1 simulations. The results are shown in Fig. 12. As observed in the experiments, curve squeal is almost completely absent in case of low adhesion (only 1 % of

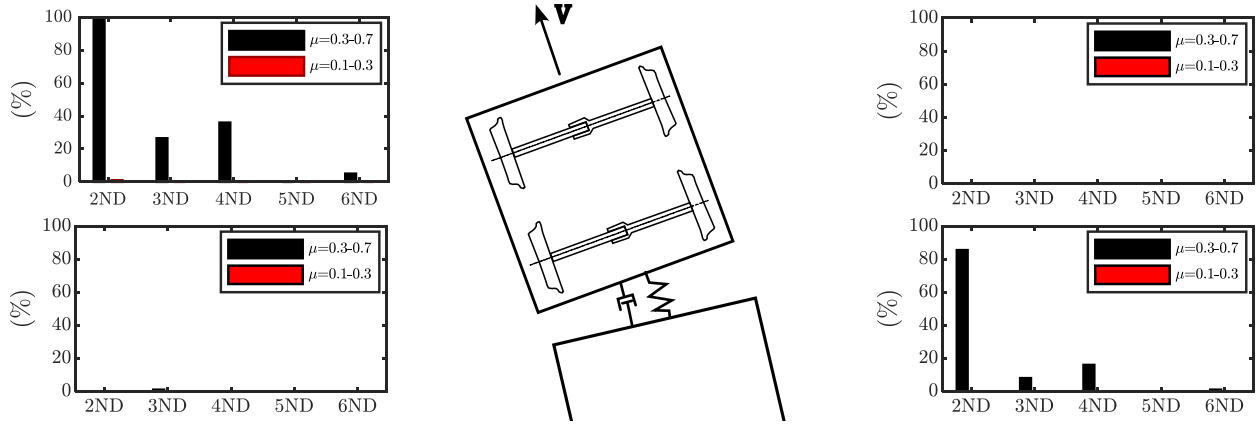

Fig. 12. Curve squeal occurrence (site 2, R = 24 m) in different adhesion conditions: (■) dry track, μ=0.3–0.7 and (■) wet track, μ=0.1–0.3.

Table 4
Summary of the experimental and numerical results for site 2.

	Dry track	Wet track
Measurements	**500,** 2500*	–
Simulations	**500,** 2500, 1500, 5100	500**

* Squeal occurrence only at curve entrance in short time windows.
** Squeal occurrence only in 1% of the simulated cases.

the inner leading wheel simulations are found unstable in proximity to the natural frequency of the wheel axial mode with 2 ND).

Table 4 provides a summary of the experimental measurements compared with the numerical results. Analogously to Table 3, the squealing frequencies from the numerical simulations are ranked according to their percentage of occurrence. For site 2 as well, good agreement is observed between the squeal frequencies measured experimentally and those obtained numerically.

4.3. Tramcar squealing behaviour under varying curve radius

The analysis is extended to examine the behaviour of the vehicle as the curve radius varies. It was previously observed that, in the case of very sharp curves, the bogies of the vehicle run under constrained curving conditions, which lead to very similar contact conditions between the wheels and, consequently, the same tendency for squeal. A parametric analysis was therefore conducted to identify whether the vehicle's behaviour differs in the case of larger curve radii. The analysis is conducted for curve radii of R = 15 m, R = 30 m, R = 45 m and R = 60 m. Squeal simulations are repeated for all the wheels of the first car, using the same friction parameters as those adopted in the previous simulations (see Table 2).

As observed in previous analyses, in the case of a very sharp curve (R = 15 m), the dynamic behaviour of the leading inner wheel is similar to that of the trailing outer wheel. Similarly, the leading outer and trailing inner wheels behave analogously. However, for larger curve radii, the behaviour of the four wheels diverges. The results of the curve squeal simulations are shown in Fig. 13. For the leading inner and trailing outer wheels, squeal occurrences decrease with increasing curve radius. A notable difference between these two wheels is that the percentage of squeal events on the trailing outer wheel drops significantly as curve radius increases. Squeal on the leading inner wheel is observed up to a curve radius of 60 m, whereas no squeal events are recorded on the trailing outer wheel beyond 45 m. This finding is consistent with reports in the literature, where wheel squeal is typically observed on the leading inner wheel of the vehicle and decreases by reducing the angle of attack between the wheel and the rail (which decreases with increasing curve radius) [1,2]. Conversely, the behaviour of the leading outer and trailing inner wheels is not straightforward. In this case, squeal occurrences slightly increase with larger curve radii. Instability is found close to the natural frequencies of the wheel modes with 3 ND, 4 ND and 5 ND. The highest squeal occurrences are found for curve radius R = 60 m on the leading outer wheel and at R = 45 m on the trailing inner wheel.

Contrary to what is observed on the leading inner and trailing outer wheels, the squeal occurrence on the other wheels, which are in flange contact, does not appear to be strictly correlated with the wheel-rail angle of attack. As observed in Section 4.1, in the case of contact between the leading inner wheel and the check rail, the mode shapes involved in instability are the ones with significant modal components in the radial direction. Therefore, the flange contact may favour mode-coupling phenomena, as also found in [17] in case of a contact point between the back of the wheel flange and the check rail. In this context, the contact angle becomes a key parameter, as also highlighted in [6,37]. The analysis conducted by Ding et al. in [6] demonstrated that the instability of specific wheel modes can be triggered by certain values of the contact angle between the wheel and the rail. The distribution of squeal probabilities observed in Fig. 13 for these two wheels can be explained by looking at the contact angle on the flange contact point as the curve radius changes (see Fig. 14a and Fig. 14b). The distribution of squeal probabilities for the two wheels is also reported. In the case of sharp curves (R = 15 m and R = 30 m) a contact angle close to 70° is observed on the flange of the two wheels. As the curve radius increases, a variation in the bogie behaviour in the curve occurs, altering the relative position between the wheels and rails. This results in a different contact angle between the two bodies. It is found that the peaks in squeal percentage (obtained at R = 45 m and R = 60 m) correspond to flange contact angles between 55° and 60°. Similar to variations in the friction coefficient, these results confirm that even seemingly minor changes in profile wear condition or wheel geometry can alter the vehicle's propensity for squeal in a specific situation.

Nevertheless, note that a higher squeal occurrence percentage does not necessarily correspond to greater noise levels. Indeed, it has been shown that the vibration amplitude during the limit cycle correlates with the steady-state creepage between the wheel and the rail (see [1,3,4,28,33]), which tends to be greater in sharp curves due to the increased angle of attack. Therefore, the noise produced during squeal

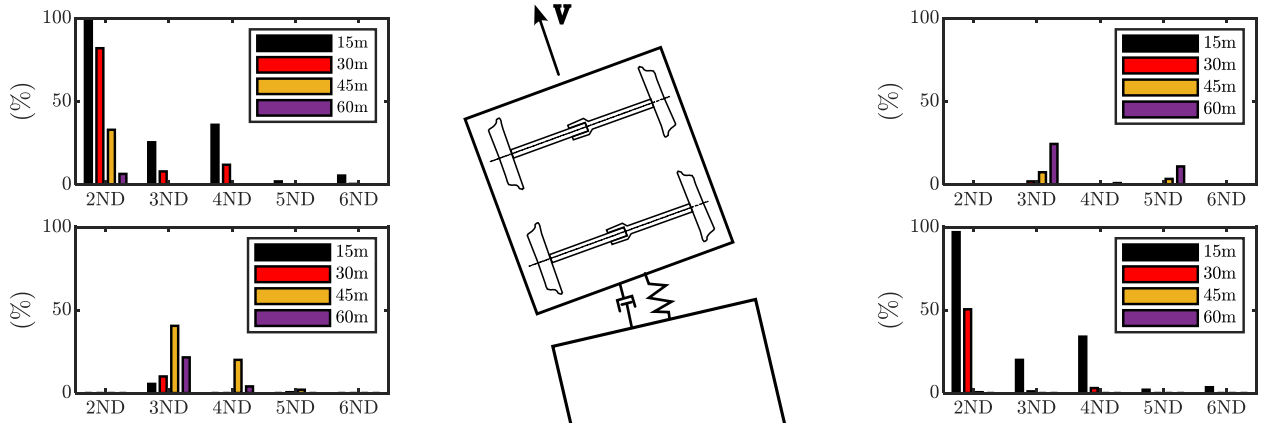

Fig. 13. Curve squeal occurrence varying the curve radius: (■) R = 15 m, (■) R = 30 m, (■) R = 45 m and (■) R = 60 m.

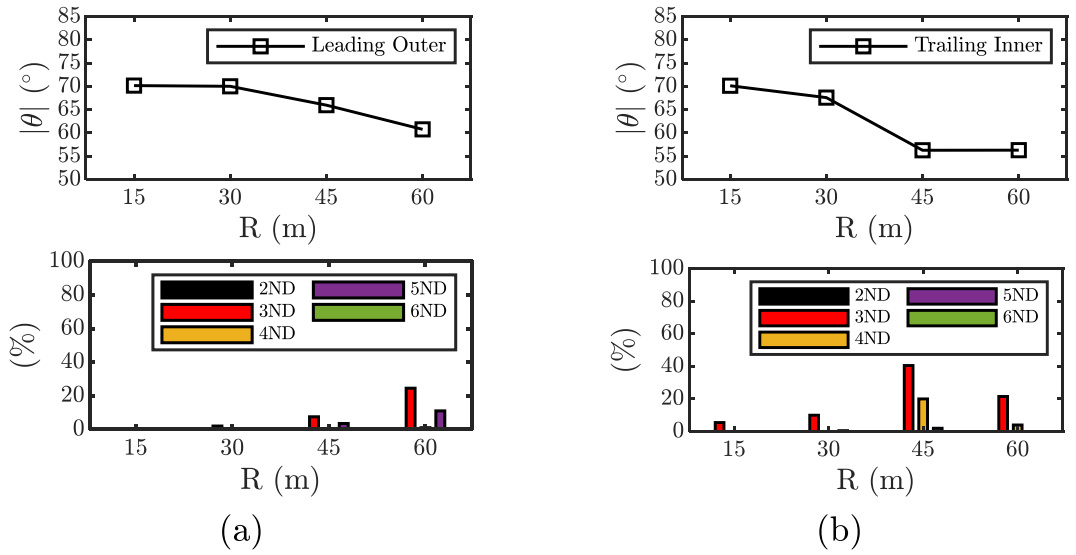

Fig. 14. Flange contact angle and squeal occurrence percentage on the (a) leading outer and (b) trailing inner wheel.

events can be significantly higher and more disturbing in the case of sharp-radius curves.

5. Discussion

The experimental analysis of noise and vibration measurements of curve squeal generated by modern low-floor tramcars at two different sites highlighted several key aspects of the phenomenon.

Measurements at site 1 revealed the intermittent nature of curve squeal through wheel vibration levels, showing that squeal can occur in various wheel vibration modes during curve negotiation. However, at any given time, a single mode dominates wheel vibration. Vibration measurements also detected curve squeal on the leading outer wheel of the same bogie.

Analysis of noise measurements at site 2 under dry and wet track conditions indicated that curve squeal can be efficiently mitigated by reducing the friction coefficient. Nevertheless, the beneficial effect of water was observed to disappear after only two vehicle passages, explaining why curve squeal is often most common immediately after rainfall. These results suggest that realistic prediction of curve squeal requires careful consideration of variability in adhesion conditions at wheel-rail contact.

Numerical analyses using vehicle dynamics simulations in the time domain and frequency-domain squeal predictions were conducted to interpret the experimental findings. Simulations are carried out considering the typical variability in wheel-rail contact conditions. The most critical wheel vibration modes are identified computing the percentage of squeal occurrence at each frequency. This shows that the frequencies observed in the experimental measurements are among the most likely to squeal predicted by the numerical model, confirming the consistency between numerical predictions and measured data.

Simulations at site 1 revealed a systematic squealing pattern across all tramcar wheels and predicted the possibility of curve squeal on leading outer wheels and trailing axles. These results corroborate the experimental evidence of multiple simultaneous squeal frequencies detected in track-side measurements. Simulations with different track gauges demonstrated that even small variations in gauge can lead to an additional contact point between the wheel flange back and the check rail, altering squeal frequencies. Furthermore, numerical simulations show that while squeal under tread contact conditions is promoted by falling friction, squeal in the case of flange or flange back contact can occur even with a constant friction coefficient. This suggests that the presence of two contact points enhances lateral-vertical dynamic coupling, leading to mode-coupling instability.

Simulations for site 2 focused on adhesion conditions and showed that low friction coefficients can effectively suppress squeal, in agreement with experimental observations on wet track.

Extending the analysis to different curve radii indicated that the leading inner wheel in sharp curves is the most critical for squeal, whereas flange contact wheels exhibited higher squeal probabilities at intermediate radii (45–60 m), depending on specific wheel-rail contact conditions. In particular, the numerical results indicate that squeal under flange contact conditions is favoured by specific values of the flange contact angle at the wheel-rail interface.

6. Conclusions

This paper presents an experimental and numerical investigation of tramcar curve squeal under varying wheel-rail contact conditions. Wheel acceleration measurements show that, although multiple vibration modes can be involved during curve negotiation, curve squeal is intermittent and typically dominated by a single mode at any given time. Tests on dry and wet tracks confirm that curve squeal can be effectively mitigated by reducing the friction coefficient, for instance through water or wheel-rail friction modifiers, yielding a reduction of nearly 15 dBA in the Single Event Level (SEL) immediately after water application. However, this mitigating effect vanishes after only two vehicle passages.

The experimental investigation is supported by a numerical procedure combining vehicle dynamics simulations and a frequency-domain model for wheel-rail interaction. The model predicts curve squeal at frequencies close to those observed experimentally. Squeal was observed in more than 90 % of the simulated cases for the front inner and rear outer wheels, while in less than 3 % of variants for the outer front wheel.

Simulations varying the friction coefficient show results consistent with the dry and wet track measurements. For friction coefficients below 0.3, squeal is observed in only about 1 % of the simulated cases, confirming the potential mitigating effect of water or friction modifiers.

Parametric analyses reveal that the most critical wheels may also depend on curve radius, with the leading inner wheel in sharp curves (radius up to 30 m) and flange-contact wheels in intermediate radii (radius up to 60 m) being most prone to squeal. It is observed that squeal in this case is promoted by specific values of the contact angle at the flange contact point.

Overall, both experimental and numerical investigations demonstrate that curve squeal is characterised by substantial variability in its

occurrence, dominant frequencies, and critical wheels, which makes reliable prediction particularly challenging.

CRediT authorship contribution statement

Federico Castellini: Writing – review & editing, Writing – original draft, Visualization, Validation, Software, Methodology, Investigation, Formal analysis, Data curation, Conceptualization. **Leonardo Faccini:** Writing – review & editing, Validation, Software, Methodology, Investigation. **Stefano Alfi:** Software, Methodology, Investigation. **Egidio Di Gialleonardo:** Writing – review & editing, Validation, Supervision, Software, Methodology, Investigation, Conceptualization. **Roberto Corradi:** Supervision, Resources, Project administration, Methodology, Investigation, Funding acquisition. **Giacomo Squicciarini:** Writing – review & editing, Validation, Supervision, Software, Methodology, Investigation, Conceptualization. **David Thompson:** Writing – review & editing, Validation, Supervision, Software, Methodology, Investigation, Conceptualization.

Declaration of competing interest

The authors declare that they have no known competing financial interests or personal relationships that could have appeared to influence the work reported in this paper.

Appendix A. . Experimental calibration of wheel and rail models

In this appendix, the procedure used to calibrate the models adopted to include the wheel and the rail dynamics in the curve squeal model is presented. The resilient wheel mounted on the reference tram has been modelled through a Finite Element (FE) software. The wheels of this tram have a nominal radius of 0.33 m and incorporate 24 V-shaped rubber elements positioned between the tyre and the web. A 3D model of the wheel has been developed adopting 159,378 brick elements (see Fig. A1). The wheel is modelled as a single body clamped in the hub, with different materials assigned to each component. The rubber elements are modelled as an equivalent rubber ring assuming a linear elastic material.

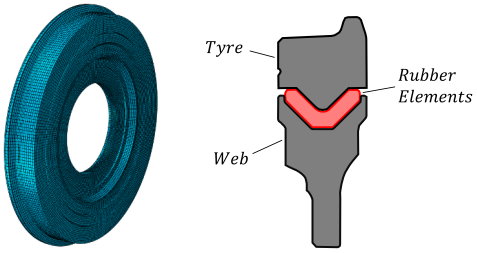

(a)

Parameter	Symbol	Units	Value
Wheel Radius	R_w	m	0.33
Steel Young Modulus	E_{steel}	MPa	210
Steel Poisson Cofficient	ν_{steel}	-	0.3
Rubber Young Modulus	E_{rubber}	MPa	36
Rubber Poisson Coefficient	ν_{rubber}	-	0.475

(b)

Fig. A1. FE model of the tramcar resilient wheel: (a) 3D model and (b) FE parameters.

An Experimental Modal Analysis (EMA) has been conducted to collect the modal parameters of the wheel up to 5 kHz, which is the frequency range of interest for curve squeal noise [1,2]. The identification of modal parameters is performed on a wheel mounted on the bogie (shown in Fig. A2), which was suspended during the experiments. The wheel dynamics is incorporated into the curve squeal model using FRFs obtained through a modal superposition approach, which combines experimentally measured natural frequencies and modal damping with numerically computed mode shapes from the finite element (FE) model. Fig. A2 compares the numerical and the experimental FRFs of the wheel in both axial and radial directions.

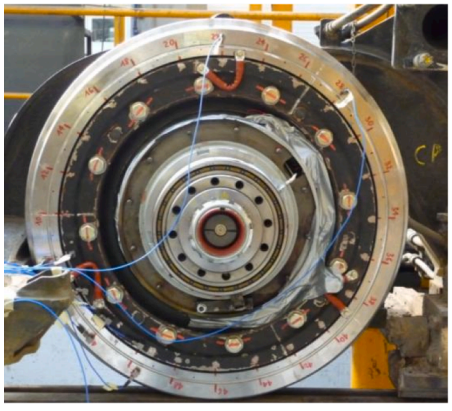

(a)

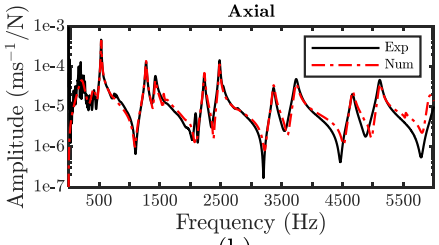

(b)

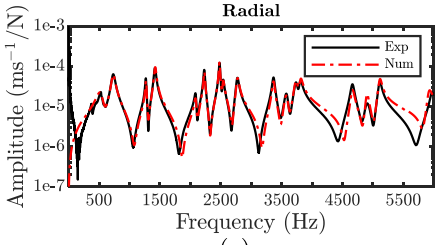

(c)

Fig. A2. EMA on the tramcar resilient wheel: (a) photograph of the instrumented wheel, (b) axial and (c) radial mobility.

The modal parameters and the wheel mode shapes associated with squealing events recorded in the experimental campaigns are reported in

Table A1. The number of Nodal Diameters (ND) for each mode is reported. As also visible in the axial and radial mobility, the mode shapes illustrated in Table A1 show that while the wheel vibration mode with 2 ND at 549 Hz is almost purely axial, the vibration modes with 3, 4 ND are strongly coupled in the two directions, such that it is difficult to distinguish properly between axial and radial modes. Consequently, the nomenclature is defined according to the direction of maximum vibration amplitude at the nominal contact point.

Table A1
Measured natural frequencies (f_n) and damping ratios (ξ_n) and predicted mode shapes (colormap refers to modal displacement magnitude) of the wheel modes with the highest curve squeal occurrence (ND = number of nodal diameters) [17].

Mode No. –	Mode Type (ND) –	Natural Frequency f_n, Hz	Damping Ratio ξ_n%	Mode Shape –
1	Axial – 2ND	535	0.80	
2	Axial – 3ND	1273	0.72	
3	Radial – 3ND	1423	1.11	
4	Web Axial – 0ND	1560	0.45	
5	Radial – 4ND	2230	0.49	
6	Axial – 4ND	2479	0.38	
7	Tyre Torsion – 1ND	2537	0.59	
8	Tyre Radial – 0ND	2774	0.76	
9	Radial – 5ND	3367	0.58	
10	Axial – 5ND	3736	0.77	
11	Axial – 6ND	5112	0.53	

The dynamics of the track is introduced in the squeal simulations through a single Timoshenko infinite beam model on a single continuous viscoelastic layer [1]. The parameters of the model are calibrated by fitting the track frequency response function obtained with impact tests on an Embedded Rail System (ERS) tramway track. A photograph of the test section and the comparison between the experimental and the numerical mobility of the track in lateral and vertical directions is shown in Fig. A3. A good match between the numerical and the experimental mobility is

obtained up to 1.5 kHz. However, the infinite beam model is still suitable for estimating the average mobility up to 5 kHz. The parameters used to calibrate the model are listed in Table A2.

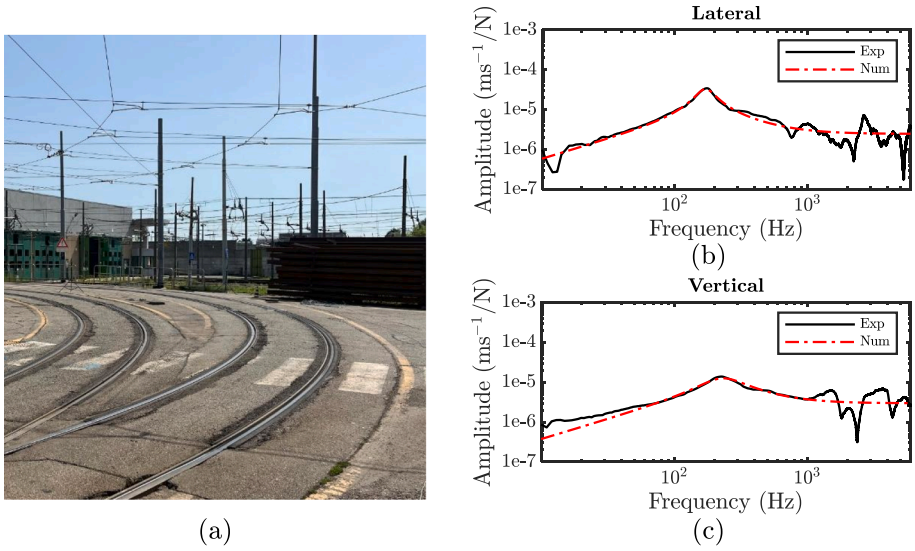

Fig. A3. Impact test on the tramway track: (a) photograph of the site, (b) lateral and (c) vertical mobility.

Table A2
Parameters used in the track model for lateral and vertical directions.

Parameter	Symbol	Unit	Value
Rail Mass*	m_r	kg/m	62
Rail Cross-Section Area	A_r	cm^2	79.45
Poisson's ratio	ν	–	0.28
Rail Shear Parameter	k	–	0.4
Rail Loss Factor	η_r	–	0.02
Rail Lateral Bending Stiffness	EI_{zz}	MNm^2	2.08
Rail Support Lateral Stiffness*	k_y	MN/m^2	70
Rail Support Lateral Loss Factor	η_y	–	0.3
Rail Vertical Bending Stiffness	EI_{yy}	MNm^2	7.07
Rail Support Vertical Stiffness*	k_z	MN/m^2	110
Rail Support Vertical Loss Factor	η_z	–	0.6

* Per unit length.

Data availability

The data that has been used is confidential.

References

[1] Thompson D. Railway Noise and Vibration: Mechanisms, Modelling and Means of Control. Elsevier, Second Edition 2024. https://doi.org/10.1016/C2012-0-07344-9.
[2] Thompson DJ, Squicciarini G, Ding B, et al. A state-of-the-art review of curve squeal noise: Phenomena, mechanisms, modelling and mitigation. Notes on Numerical Fluid Mechanics and Multidisciplinary Design 2018;139:3–41.
[3] Huang Z. Theoretical modelling of railway curve squeal. University of Southampton; 2007. PhD thesis.
[4] Hsu SS, Huang Z, Iwnicki SD, et al. Experimental and theoretical investigation of railway wheel squeal. Proc Inst Mech Eng F J Rail Rapid Transit 2007;221(1):59–73.
[5] Xie G, Allen PD, Iwnicki SD, et al. Introduction of falling friction coefficients into curving calculations for studying curve squeal noise. Veh Syst Dyn 2006;44:261–71.
[6] Ding B, Squicciarini G, Thompson D, et al. An assessment of mode-coupling and falling-friction mechanisms in railway curve squeal through a simplified approach. J Sound Vib 2018;423:126–40.
[7] Meehan PA. Prediction of wheel squeal noise under mode coupling. J Sound Vib 2020;465.
[8] Liu S, De Silva U, Chen D, et al. Investigation of wheel squeal noise under mode coupling using two-disk testrig experiments. Wear 2023;530–531:205035.
[9] Hoffmann N, Fischer M, Allgaier R, et al. A minimal model for studying properties of the mode-coupling type instability in friction induced oscillations. Mech Res Commun 2002;29(4):197–205.
[10] Ding B, Squicciarini G, Thompson D. Effect of rail dynamics on curve squeal under constant friction conditions. J Sound Vib 2019;442:183–99.
[11] Lai VV, Chiello O, Brunel JF, et al. The critical effect of rail vertical phase response in railway curve squeal generation. Int J Mech Sci 2020;167.
[12] Kropp W, Theyssen J, Pieringer A. The application of dither to mitigate curve squeal. J Sound Vib 2021;514:116433.
[13] Heckl MA, Abrahams ID. Curve squeal of train wheels, Part 1: mathematical model for its generation. J Sound Vib 2000;229(3):669–93.
[14] Heckl MA. Curve squeal of train wheels, Part 2: which wheel modes are prone to squeal? J Sound Vib 2000;229(3):695–707.
[15] De Beer FG, Janssens MHA, Kooijman PP. Squeal noise of rail-bound vehicles influenced by lateral contact position. J Sound Vib 2003;267(3):497–507.
[16] Squicciarini G, Usberti S, Thompson DJ, et al. Curve Squeal in the Presence of two Wheel/Rail Contact Points. Notes on Numerical Fluid Mechanics and Multidisciplinary Design Springer 2015:603–10.
[17] Castellini F, Faccini L, Di Gialleonardo E, et al. Curve squeal in sharp curves: effect of multiple wheel/rail contact points. Appl Acoust 2024;218.
[18] Macfarlane AGJ, Postlethwaite I. The generalized nyquist stability criterion and multivariable root loci. Int J Control 1977;25(1):81–127.
[19] Caverly RJ, Pates R, Bridgeman LJ, et al. MIMO Nyquist interpretation of the large gain theorem. Int J Control 2020;93(10):2326–35.

[20] Liu X, Ye S, Mei C. Investigation of the effect of longitudinal creepage on wheel squeal. JVC/Journal of Vibration and Control 2023. https://doi.org/10.1177/10775463231186298.
[21] Feng X, Chen G, Song Q, et al. A root Cause of Curve Squeal: Self-Excited Frictional Vibration of a Wheelset–Track System. J Tribol 2024;146(6).
[22] Feng X, Chen G, Song Q, et al. Comparison of modeling methods and mitigation measures for curve squealing. JVC/Journal of Vibration and Control 2025;31(11–12):2424–38.
[23] Feng X, Chen G, Dong B. Study on the Mechanism of Outer Wheel Squeal on Subway Large-Radius Curves. Tribol Trans 2025. https://doi.org/10.1080/10402004.2025.2479074.
[24] Chongyi C, Chengguo W, Ying J. Study on numerical method to predict wheel/rail profile evolution due to wear. Wear 2010;269(3–4):167–73.
[25] Łuczak B, Firlik B, Staśkiewicz T, et al. Numerical algorithm for predicting wheel flange wear in trams – Validation in a curved track. Proc Inst Mech Eng F J Rail Rapid Transit 2020;234(10):1156–69.
[26] Liu X, Meehan PA. Investigation of the effect of lateral adhesion and rolling speed on wheel squeal noise. Proc Inst Mech Eng F J Rail Rapid Transit 2013;227(5):469–80.
[27] Liu X, Meehan PA. Investigation of squeal noise under positive friction characteristics condition provided by friction modifiers. J Sound Vib 2016;371:393–405.
[28] Meehan PA, Liu X. Modelling and mitigation of wheel squeal noise amplitude. J Sound Vib 2018;413:144–58.
[29] Meehan PA, Liu X. Modelling and mitigation of wheel squeal noise under friction modifiers. J Sound Vib 2019;440:147–60.
[30] Meehan PA, Liu X. Wheel squeal noise control under water-based friction modifiers based on instantaneous rolling contact mechanics. Wear 2019;440:203052.
[31] Chiello O, Ayasse JB, Vincent N, et al. Curve squeal of urban rolling stock-Part 3: Theoretical model. J Sound Vib 2006;293(3):710–27.
[32] Giner-Navarro J, Martínez-Casas J, Denia FD, et al. Study of railway curve squeal in the time domain using a high-frequency vehicle/track interaction model. J Sound Vib 2018;431:177–91.
[33] Lai VV, Anciant M, Chiello O, et al. A nonlinear FE model for wheel/rail curve squeal in the time-domain including acoustic predictions. Appl Acoust 2021;179.
[34] Pieringer A. Time-domain modelling of high-frequency wheel/rail interaction. Chalmers University of Technology; 2011. PhD thesis.
[35] Pieringer A. A numerical investigation of curve squeal in the case of constant wheel/rail friction. J Sound Vib 2014;333(18):4295–313.
[36] Zenzerovic I, Kropp W, Pieringer A. An engineering time-domain model for curve squeal: Tangential point-contact model and Green's functions approach. J Sound Vib 2016;376:149–65.
[37] Zenzerovic I, Kropp W, Pieringer A. Influence of spin creepage and contact angle on curve squeal: a numerical approach. J Sound Vib 2018;419:268–80.
[38] Corradi R, Crosio P, Manzoni S, et al. Experimental investigation on squeal noise in tramway sharp curves. Proceedings of the 8th International Conference on Structural Dynamics, EURODYN. 2011;3214–21.
[39] Torstensson PT, Pieringer A, Höjer M, et al. A case study of railway curve squeal radiated from both the outer and inner wheel. Appl Acoust 2025;228:110327.
[40] Castellini F, Faccini L, Di Gialleonardo E, et al. Predictive Modelling of Curve Squeal Occurrence in Tramways: Influence of Wheel/Rail double contact Points. Noise and Vibration Mitigation for Rail Transportation Systems Springer 2024:501–9.
[41] Monk-Steel AD, Thompson DJ, de Beer FG, et al. An investigation into the influence of longitudinal creepage on railway squeal noise due to lateral creepage. J Sound Vib 2006;293(3–5):766–76.
[42] Castellini F, Faccini L, Di GE, et al. Curve squeal of modern tramcars: comparison between independently rotating wheels and solid axles. International Journal of Rail Transportation 2024;1–18.
[43] Corradi R, Facchinetti A, Manzoni S, et al. Effects of track parameters and environmental conditions on tramcar induced squeal noise. In: ISMA2006: International Conference on Noise and Vibration Engineering; 2006. p. 3745–59.
[44] Eadie DT, Santoro M. Top-of-rail friction control for curve noise mitigation and corrugation rate reduction. J Sound Vib 2006;293(3–5):747–57.
[45] Eadie DT, Santoro M, Powell W. Local control of noise and vibration with KELTRACK^{TM} friction modifier and Protector® trackside application: an integrated solution. J Sound Vib 2003;267(3):761–72.
[46] Castellini F, Faccini L, Alfi S, et al. The influence of wheel/rail contact conditions on curve squeal noise: experimental and numerical investigation. Prague: Development and Maintenance; 2024.
[47] En BS. 61672-1:Electroacoustics. Sound level meters -. Specifications 2013.
[48] Polach O. Creep forces in simulations of traction vehicles running on adhesion limit. Wear 2005;258(7–8):992–1000.
[49] Iso. Acoustics railway applications measurements of noise emitted by railbound vehicles 2013;3095::2013.
[50] Cheli F, Corradi R, Diana G, et al. Validation of a numerical model for the simulation of tramcar vehicle dynamics by means of comparison with experimental data. J Comput Nonlinear Dyn 2007;2(4):299–307.
[51] Corradi R, Diana G, Facchinetti A. Sharp curve negotiation analysis of tramcar vehicles with different bogie architectures. Civil-Comp. Proceedings 2012;98.
[52] Belforte P, Cheli F, Corradi R, et al. Software for the numerical simulation of tramcar vehicle dynamics. Heavy Vehicle Systems 2003;10(1–2):48–69.
[53] Cheli F, Corradi R, Facchinetti A. A numerical model to analyse the dynamic behaviour of modern tramcars. In: Proceedings of the Mini Conference on Vehicle System Dynamics, Identification and Anomalies; 2002. p. 183–90.
[54] Pascal JP, Sauvage G. The Available Methods to Calculate the Wheel/Rail Forces in Non Hertzian Contact Patches and Rail Damaging. Veh Syst Dyn 1993;22(3–4):263–75.
[55] Bruni S, Collina A, Diana G, et al. Lateral dynamics of a railway vehicle in tangent track and curve: Tests and simulation. Veh Syst Dyn 2000;33(SUPPL.):464–77.
[56] Polach O. A Fast Wheel-Rail Forces Calculation Computer Code. Veh Syst Dyn 1999;33:728–39.
[57] Giménez JG, Alonso A, Gómez E. Introduction of a friction coefficient dependent on the slip in the FastSim algorithm. Veh Syst Dyn 2005;43(4):233–44.
[58] Der KK. einfluß der fahrgeschwindigkeit auf den haftwert zwischen rad und schiene. Arch für Eisenbahntechnik 1967;22:58–78.
[59] Lewis R, Olofsson U. Wheel-rail interface handbook. Elsevier Ltd: Wheel-Rail Interface Handbook; 2009.
[60] Knothe K, Stichel S. Rail vehicle dynamics. Rail Vehicle. Dynamics 2016:1–321.